Heat Transfer and Fluid Flow in the Welding Arc

J. McKELLIGET and J. SZEKELY

Through the numerical solution of the Navier/Stokes equation, the energy transport equation, and the magnetic diffusion equation, a mathematical model has been developed to predict the velocity, temperature, and current density distributions in inert gas welding arcs. Although the model has one adjustable parameter, the cathode current density, it was found that a single value of this variable was sufficient to provide internally consistent results for a range of arc lengths and arc currents representative of welding. The computed temperature distributions in the arc were found to be in good agreement with spectroscopically measured temperatures taken from the literature, and similar agreement was obtained between the predicted and measured current density distributions at the surface of water cooled copper anodes. The mechanisms of heat and momentum transfer to the anode were investigated in the light of recent findings concerning the anode boundary layer and the presence of negative anode fall voltages. The predicted convective heat fluxes to the anode were found to be generally consistent with experimental data.

I. INTRODUCTION

THE purpose of the work described in this paper is to develop a quantitative representation of heat and fluid flow phenomena in welding arcs, with particular reference to the interface between the arc and the bounding surfaces. The main motivation for this work is provided by recent research into weldpool behavior.[1]

In modeling the electromagnetic, heat and fluid flow phenomena in weldpools, the interaction between the welding arc and the weldpool appears as boundary conditions. Up to the present these boundary conditions were introduced on an empirical basis. Ultimately it would be highly desirable to represent arc welding systems in terms of a formulation where the transport phenomena in the arc and in the pool are fully and interactively coupled. The present work represents a useful intermediate step in this direction by allowing an explicit definition of the interaction of an impinging plasma jet with a solid surface.

In recent years there has been considerable interest in representing the electromagnetic heat and fluid flow phenomena in DC plasma arcs. Work in this laboratory has involved the study of high current arcs, with emphasis on turbulence phenomena and on the overall behavior of the system.[2,3,4] The interesting and useful work carried out by Pfender and his associates[5,6] involved the direct incorporation of experimental measurements in their models. More specifically, in modeling heat flow phenomena the boundary conditions for temperature at the anode surface were deduced from experimental measurements.

The work to be described in this paper differs from previous research because it seeks to develop a general, internally self-consistent engineering representation of the system, without recourse to empiricism.

J. McKELLIGET is Assistant Professor, Department of Mechanical Engineering, University of Lowell, Lowell, MA 01854. J. SZEKELY is Professor of Materials Engineering, Department of Materials Science and Engineering, Massachusetts Institute of Technology, Cambridge, MA 02139.

Manuscript submitted January 31, 1985.

II. MODEL FORMULATION

The presence of an electric field between the cathode and the weldpool (anode), sketched in Figure 1, causes the passage of an electric current through the ionized plasma region which, in turn, gives rise to a self-induced magnetic field. The magnetic field interacts with the current transferring momentum to the gas, which is accelerated toward the anode in the form of the characteristic cathode jet. Due to the electrical resistance of the plasma, the energy produced by the current maintains the plasma in the ionized state and provides the heating mechanism for the welding process. In modeling the system the following simplifying assumptions have been made:

1. The arc is radially symmetric and the governing equations take a two dimensional form when expressed in terms of cylindrical polar coordinates.

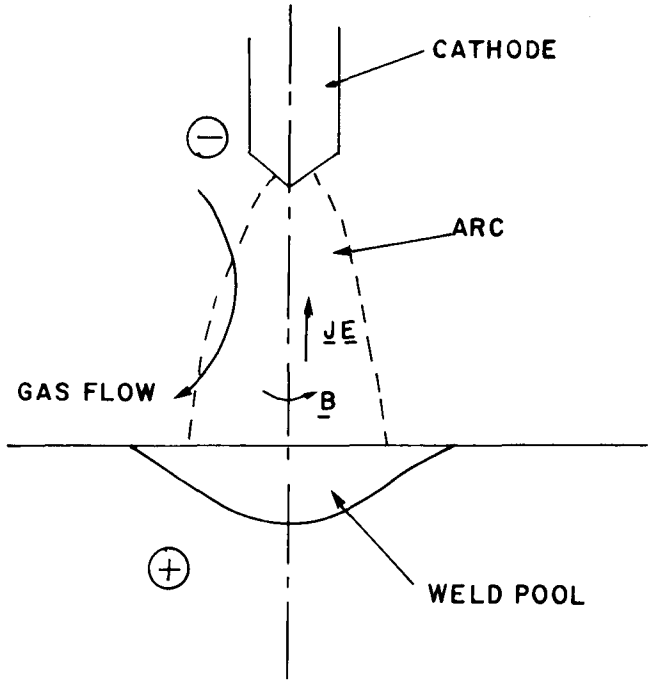

Fig. 1 — Schematic representation of the arc and weldpool region.

2. The arc is steady and hence the governing equations take a time-independent form. Essentially the requirement for this assumption to be valid is that the residence time of the working gas in the arc should be much less than the period of any fluctuations imposed upon the system. Taking a typical arc velocity of 100 m/s and an arc length of 10 mm, the gas residence time is about 0.1 ms which is much shorter than any externally imposed fluctuations.
3. The arc is in Local Thermodynamic Equilibrium (LTE) which means that the electron and heavy particle temperatures are equal. The recent work of Hsu and Pfender[5,6] has compared predictions based upon a two-temperature and a one-temperature model of the welding arc. They found that the assumption of LTE is excellent over most of the arc with significant deviations occurring only in the cooler arc fringes and in the immediate vicinity of the anode.
4. The arc gas is taken to be pure argon at 1 atmosphere. This neglects the presence of metal vapor contaminants produced by the electrodes (*i.e.*, nonconsumable electrodes) and the presence of the surrounding atmosphere.
5. The flow is laminar. Taking the characteristic velocity as 100 m/s, the characteristic length as 0.01 m, and the kinematic viscosity of argon at 20,000 K as 1.9 g/m-s, gives a Reynolds number of 520. Since the transition to turbulence for a free jet occurs at a Reynolds number of about 100,000, the flow may sensibly be considered to be laminar.
6. The plasma is optically thin and the radiation may be modeled in an approximate manner by defining a radiation loss per unit volume.
7. A flat cathode will be assumed. This assumption is included for computational convenience only and is somewhat unsatisfactory since a pointed cathode is generally used in arc welding. An indication of the influence of the electrode tip angle is provided by the work of Tsai[7] who found that the anode current density increased by about 25 pct when the tip angle was decreased from 120 to 30 deg. It is evident, therefore, that the assumption of a flat electrode should be relaxed in future calculations. This has been achieved by Hsu *et al.*[5] for the calculation of the temperature and velocity fields but not for the calculation of the electromagnetic field.

Under the above assumptions the equations governing the arc region may be written as follows:

Equation of mass continuity:

$$\frac{\partial}{\partial z}(\rho u) + \frac{1}{r}\frac{\partial}{\partial r}(\rho r v) = 0 \qquad [1]$$

Conservation of axial momentum:

$$\frac{\partial}{\partial z}(\rho u^2) + \frac{1}{r}\frac{\partial}{\partial r}(\rho r v u) = -\frac{\partial P}{\partial z} + \frac{2\partial}{\partial z}\left(\mu\frac{\partial u}{\partial z}\right) + \frac{1}{r}\frac{\partial}{\partial r}\left\{r\mu\left(\frac{\partial u}{\partial r} + \frac{\partial v}{\partial z}\right)\right\} + F_z \qquad [2]$$

Conservation of radial momentum:

$$\frac{\partial}{\partial z}(\rho u v) + \frac{1}{r}\frac{\partial}{\partial r}(\rho r v^2) = -\frac{\partial P}{\partial r} + \frac{\partial}{\partial z}\left\{\mu\left(\frac{\partial v}{\partial z} + \frac{\partial u}{\partial r}\right)\right\} + \frac{2}{r}\frac{\partial}{\partial r}\left(\mu\frac{r\partial v}{\partial r}\right) - \frac{2v}{r^2}\mu + F_r \qquad [3]$$

Conservation of energy:

$$\frac{\partial}{\partial z}(\rho u h) + \frac{1}{r}\frac{\partial}{\partial r}(\rho r v h) = \frac{\partial}{\partial z}\left\{\frac{k}{C_p}\frac{\partial h}{\partial z}\right\} + \frac{1}{r}\frac{\partial}{\partial r}\left\{\frac{kr}{C_p}\frac{\partial h}{\partial r}\right\} + S_t \qquad [4]$$

In these equations z and r are the axial and radial coordinates, respectively, which are defined in Figure 2. The left-hand sides of Eqs. [2], [3], and [4] represent the convective transport of momentum and enthalpy caused by the motion of the fluid, while the right-hand sides represent diffusive transport due to molecular motion, and also the source terms per unit volume. Although a temperature dependent density is included in the model, gas compressibility effects have been neglected since the plasma velocities are well into the subsonic region.

F, the Lorentz force driving the flow, is defined by the following equation:

$$\mathbf{F} = \mathbf{J} \times \mathbf{B} \qquad [5]$$

where **J** is the current density, and **B** is the self-induced magnetic field in the arc.

The source term in the energy equation may be expressed as

$$S_t = \left(\frac{J_z^2 + J_r^2}{\sigma}\right) - S_r - \frac{5}{2}\frac{k_B}{e}\left\{\frac{J_z}{C_p}\frac{\partial h}{\partial z} + \frac{J_r}{C_p}\frac{\partial h}{\partial r}\right\} \qquad [6]$$

The first term represents the Joule heating caused by the arc resistance, S_r is the optically thin radiation loss per unit volume, and the final term represents the enthalpy transported by the electrons due to the fact that the electron velocity is generally much higher than the heavy particle velocity. The radiation loss for argon was taken from the work of Evans and Tankin,[8] and the remaining plasma properties were taken from the tabulated data of Liu.[9]

In addition to the above equations it is necessary to solve Maxwell's equations for the electromagnetic field. In the present work we have chosen to solve the magnetic diffusion equation for the azimuthal magnetic field, B, which

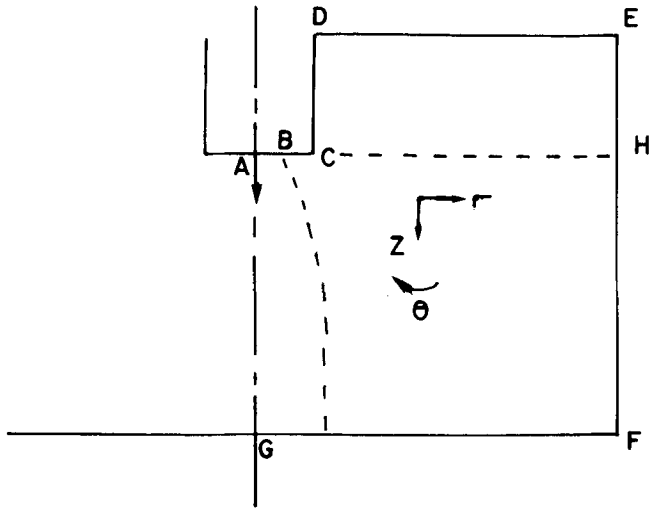

Fig. 2—Integration region (ABCDEFG) and the coordinate system, (r, z, θ).

in the absence of electromagnetic induction terms may be written as:

$$\frac{\partial}{\partial z}\left\{\sigma\frac{1}{(T)}\frac{\partial B}{\partial z}\right\}+\frac{\partial}{\partial r}\left\{\sigma\frac{1}{(T)r}\frac{\partial}{\partial r}(rB)\right\}=0 \qquad [7]$$

with the additional relationships

$$\mu_0 J_z=\frac{1}{r}\frac{\partial}{\partial r}(rB), \qquad \mu_0 J_r=-\frac{\partial B}{\partial z} \qquad [8]$$

for the current density.

A sketch of the integration region is given in Figure 2 and the corresponding boundary conditions are given in Table I. These express the conditions of zero velocity at solid surfaces and zero fluxes across the axis of symmetry. The boundaries DE and EF are taken to be at large distances from the arc and to have little effect on the plasma region.

A special treatment is required for the two solid boundaries corresponding to the anode and cathode since deviations from LTE may occur in these regions.

(i) *Cathode Region*

A major problem encountered when solving the governing equations in the vicinity of the cathode is that very little is known concerning the transition from the relatively cool electrode to the hot plasma column. In the classical model an electrical sheath is postulated between the plasma and the electrode and strong electric fields accelerate the electrons, produced by thermionic emission at the cathode, across this sheath and into the plasma.

In a recent investigation of the cathode region, Hsu and Pfender[10] have demonstrated that while the heavy particle temperature decreases rapidly to the cathode temperature as the surface of the electrode is approached, the electron temperature maintains a comparatively high temperature up to the edge of the cathode sheath. Thus, in calculating the electron enthalpy in the vicinity of the cathode spot the electrons are characterized by the temperature of the plasma column adjacent to the electrode, $T_{e,c}$ rather than by the cathode temperature itself.

If we assume that the electrons are in "free fall" across the sheath then we may include this effect by defining a cathode fall voltage, V_c, through the relation

$$eV_c = 5/2\ k_B T_{e,c} \qquad [9]$$

In this expression a plasma column temperature of 20,000 K is equivalent to a cathode fall of 4.3 V. Although this is certainly an over-simplification of the processes occurring in the cathode fall zone, it does permit an approximate allowance for the contribution of the cathode fall voltage to the total arc power.

In effect the present model solves the governing equations up to the edge of the cathode sheath rather than to the electrode itself. Since the sheath thickness is of the order of the Debye length (which for an argon plasma at atmospheric pressure is around 10^{-4} mm), the edge of the sheath and the cathode surface may be taken as coincident. Other mechanisms of enthalpy transport between the plasma region and the cathode (*e.g.*, convective losses from the plasma) are set equal to zero in the model since they are considerably less than the electron enthalpy term.

The boundary condition for B along the lower surface of the cathode (AH) is obtained by assuming that the current density there takes a constant value, J_c, inside the cathode spot and is zero outside. *i.e.*:

$$J_z = J_c, \qquad r < R_c$$
$$J_z = 0, \qquad r > R_c \qquad [10]$$

where R_c is the cathode spot radius which is given by the relation,

$$R_c=\left\{\frac{I}{\pi J_c}\right\}^{0.5} \qquad [11]$$

Combining Eqs. [8] and [10] it is possible to calculate B at the surface of the cathode explicitly, *i.e.*:

$$B = \mu_0 Ir/(2\pi R_c^2) \qquad r < R_c$$
$$B = \mu_0 I/(2\pi r) \qquad r > R_c \qquad [12]$$

The model still requires that the unknown parameter, J_c, be specified. The measurement of this parameter (*via* the cathode spot radius) is very difficult because of the intense radiation emitted by the plasma in the vicinity of the cathode tip and its calculation would require a model of the cathode fall zone, heat transfer within the cathode, as well as reliable data on the electrode work function. In the present model J_c is used as an adjustable parameter which may be varied until the correct arc voltage is obtained and the predicted temperature contours are in agreement with experiment. This is not as arbitrary as it may seem at first since it was found that a single value of the cathode current density gave good agreement with experimental measurements for different values of the arc current and arc length. Indeed, a single value (65 A/mm^2) has been used throughout this study.

(ii) *Anode*

Figure 3 shows the principal mechanisms which contribute to heat transfer from the plasma jet to the anode: heat transfer by convection, heat transfer due to the electron

Table I. Boundary Conditions

	u	v	h	B
AB	0	0	$T = 1000$ K $Q = \lvert J_z \rvert V_c$	$\frac{\mu_0 Ir}{2\pi R_c^2}$
BC	0	0	$\frac{\partial h}{\partial z} = 0$	—
CD	0	0	$\frac{\partial h}{\partial r} = 0$	—
DE	$\frac{\partial}{\partial z}(\rho u) = 0$	0	$T = 1000$ K	—
EF	$\frac{\partial u}{\partial r} = 0$	$\frac{\partial v}{\partial r} = 0$	$T = 1000$ K	$\frac{\mu_0 I}{2\pi r}$
GF	0	0	$T = 1000$ K Eq. [16]	$\frac{\partial B}{\partial z} = 0$
AG	$\frac{\partial u}{\partial r} = 0$	0	$\frac{\partial h}{\partial r} = 0$	$B = 0$
BH	—	—	—	$\frac{\mu_0 I}{2\pi r}$

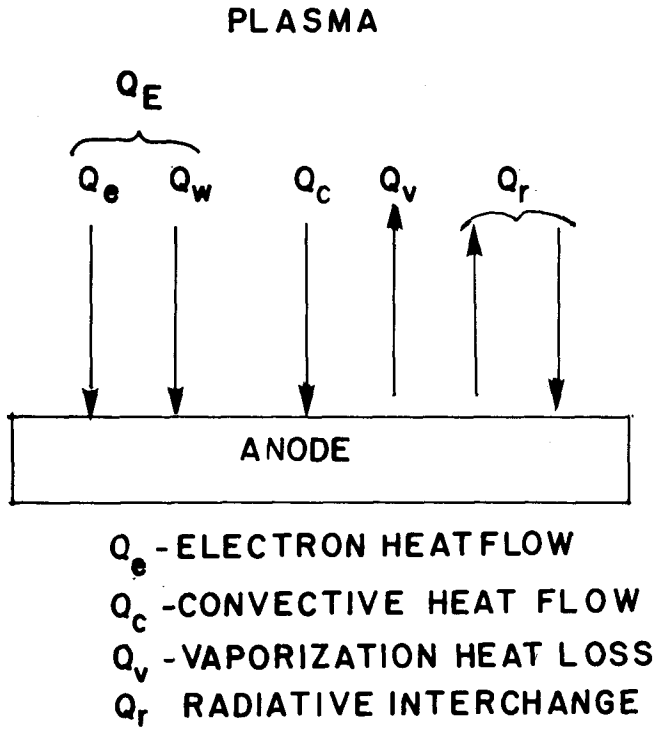

Fig. 3—Anode heating mechanisms.

flow, heat transfer by radiation both from the plasma and from the anode, and heat loss due to vaporization of the anode material.

The classical theory of heat transfer to the anode of high intensity arcs is similar to the corresponding theory of the cathode with the presence of an electrical sheath across which there exists a positive voltage drop (the anode fall voltage V_a).

The heat flux to the anode due to the flow of electrons may then be expressed as:

$$Q_E = J_a\left\{5/2 + \frac{e\phi}{k_B\sigma}\right\} k_B T_{e,a}/e + J_a V_w + J_a V_a \qquad [13]$$

The first term is the transport of enthalpy due to the random thermal energy of the electrons, the Thomson effect, while the second term represents the heat given up by the electrons as they enter the lattice of the anode and release energy proportional to the anode work function. The third term is the energy acquired by the electrons in traversing the anode fall. In principle, this energy is required in order to sustain the production of positive ions in the vicinity of the anode and to ensure current conservation. If field ionization is the governing mechanism, this would require anode falls of tens of volts which is inconsistent with experimental measurements suggesting anode falls of only a few volts.

In a recent paper Dinulescu and Pfender[11] proposed a model of the anode boundary layer which takes into account diffusion effects. They predicted that while the temperature of the heavy particles (atoms and positive ions) approached the temperature of the anode, the electrons maintained a relatively high temperature (~10,000 K) ensuring a conducting path to the anode. In addition, they predicted that the anode fall voltage would become negative due to a surplus of electrons near the surface of the electrode.

In a later paper Sanders and Pfender[12] reported on measurements of the anode fall voltage for water cooled copper targets and for arc currents in the range 100 to 250 A using an electric probe. They confirmed the predictions of Dinulescu and Pfender[11] and found that the anode fall voltage varied from −2.1 to −1.4 V. These results have important consequences for the anode heat transfer mechanism since the directed energy eV_a that the electrons would acquire from a positive anode fall must now be eliminated from the anode energy balance.

The electron energy flux to the anode may now be written as:

$$Q_E = J_a\left\{5/2 + \frac{e\phi}{k_B\sigma}\right\} k_B T_{e,a}/e + J_a V_w \qquad [14]$$

where ϕ is the coefficient of thermal diffusion for the electrons. Dinulescu and Pfender[11] have demonstrated that the term in parentheses may (for an argon plasma with electron temperatures above 10,000 K) be replaced by the constant value 3.203.

Since the present model is based upon the assumption of LTE, it is not possible to calculate the electron temperature at the anode explicitly. However, it has been shown[11] that near the arc root on the anode the electron temperature is approximately 10,000 K and hence it is possible to simplify further the electron energy flux as,

$$Q_E = J_a\{2.76 + V_w\} \qquad [15]$$

Q_C: The convective heat transfer term can be divided into a true convective contribution caused by the motion of the plasma past the anode and a purely conductive term which would exist even if the plasma were at rest.

The convective contribution depends upon the arc current and the electrode separation. At high currents or small arc lengths an appreciable cathode jet exists at the anode and the flow in the vicinity of the electrode becomes an impinging jet flow (cathode jet dominated mode). At lower currents or larger separations the strength of the cathode jet is considerably diminished and the contraction of the arc in the region of the anode results in the formation of an anode jet directed away from the anode and toward the cathode (anode jet dominated mode). Since the velocities in the anode jet are much less than those in the cathode jet, pure convective heating is negligible in this mode of operation.

The convective heat transfer may be found in two ways: by solving for the temperature in the boundary layer and evaluating the flux at the wall, or by the use of approximate heat transfer correlations which require a knowledge of conditions at the edge of the boundary layer and at the wall only. In the present paper we used the second approach since it does not require a two temperature model of the anode boundary layer. A heat transfer correlation for impingement flow of argon was taken from the literature[13] and may be written as:

$$Q_C = \frac{0.515}{\alpha_a}\left(\frac{\mu_b\rho_b}{\mu_a\rho_a}\right)^{0.11}\left\{\mu_a\rho_a\frac{dv}{dr}\right\}^{0.5}(h_b - h_a) \qquad [16]$$

This correlation was derived from reentry problem studies and is valid for reentry speeds up to 9000 m/s which corresponds to a stagnation enthalpy of 4×10^7 J · kg^{-1} (T ~ 15,000 K for argon).

Q_r: The final contribution to the anode heat flux considered was due to radiation from the plasma. This was calculated by using approximate view factors. The radiative flux received by surface element i from volume element j (see Figure 4) may be obtained from the following relationship:

$$Q_{r,i,j} = \int_{v_j} \frac{S_r}{4\pi r_{i,j}^2} \cos \psi \, dv_j \qquad [17]$$

This integral was evaluated approximately for each surface and volume element of the finite difference mesh by assuming that the element could be assigned a constant value of r and z. This treatment should be sufficiently accurate for most regions except those very close to the anode.

Heat loss through evaporation of the anode material was taken as zero in the present paper since only water cooled targets were considered. It should be noted, however, that under real welding conditions vaporization from the weld-pool does make an appreciable contribution to the overall heat balance.

In conclusion, the anode heat flux may be written in the simplified form:

$$Q(r) = J_a(r)\{2.76 + V_w\} + Q_C(r) + Q_r(r) \qquad [18]$$

The boundary condition imposed upon B at the anode, that its normal spatial derivative be zero, corresponds to a requirement that there be no radial current fluxes at the surface.

III. TECHNIQUE OF SOLUTION

The governing equations were solved numerically using a finite difference procedure described by Pun and Spalding.[14]

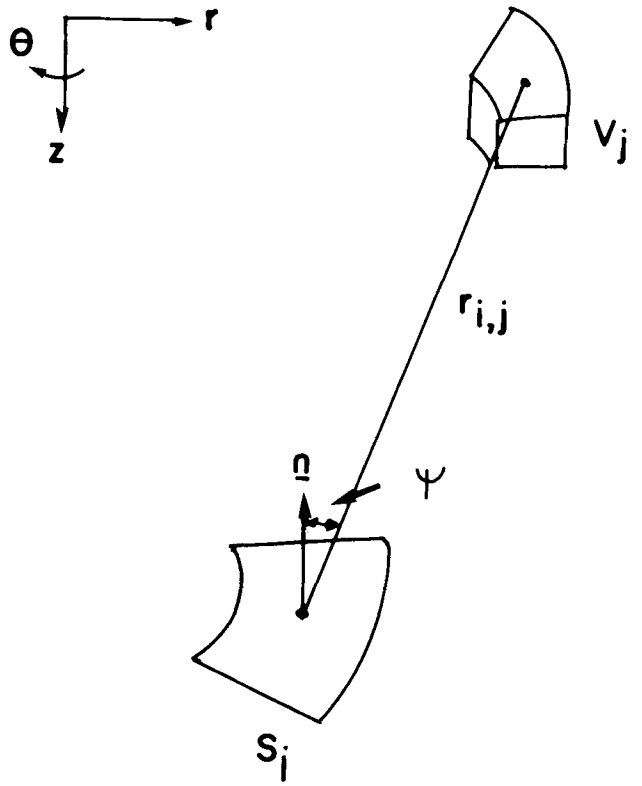

Fig. 4—Configuration factor geometry.

The finite difference equations were solved iteratively until a steady, qualitatively correct solution was obtained and until the overall mass and energy balances were satisfied to within 95 pct. A 20 × 23 grid was used and the calculations required about 10 minutes of CPU time on the IBM 370 computer.

IV. COMPUTED RESULTS

The model was run for 100 A and 200 A arcs for a variety of arc lengths. A cathode current density of 65 A/mm^2 was used for all the runs. This corresponded to a cathode spot radius of 0.7 mm for the 100 A arcs and 1 mm for the 200 A arcs.

(i) *Temperature*

The predicted temperatures for 10 mm arcs at 100 A and 200 A are shown in Figures 5 and 6, respectively, along with the experimental temperature measurements of Hsu *et al.*[5] The predicted temperatures for the 100 A arc are generally slightly higher than the measurements but there appears to be quite good overall agreement. A similar situation exists for the 200 A arc except that the maximum predicted temperature is closer to the maximum observed temperature.

Figure 7 shows the predicted axial temperatures corresponding to Figures 5 and 6. The two curves have almost the same shape but the absolute values differ by about 2000 K.

The predicted arc voltages for these conditions were 13.2 and 14.1 V, respectively. These are somewhat less than measured values of 14.3 V at 100 A[7] and 16 V at 200 A.[15] The discrepancies may well result from an underestimation of the cathode fall voltages which were calculated to be 3.6 V and 3.56 V, respectively.

(ii) *Velocity*

The calculated velocity field for the 200 A arc is shown in vector form in Figure 8. Although there are no experimental measurements with which to compare the calculations directly, they serve to show the general nature of the

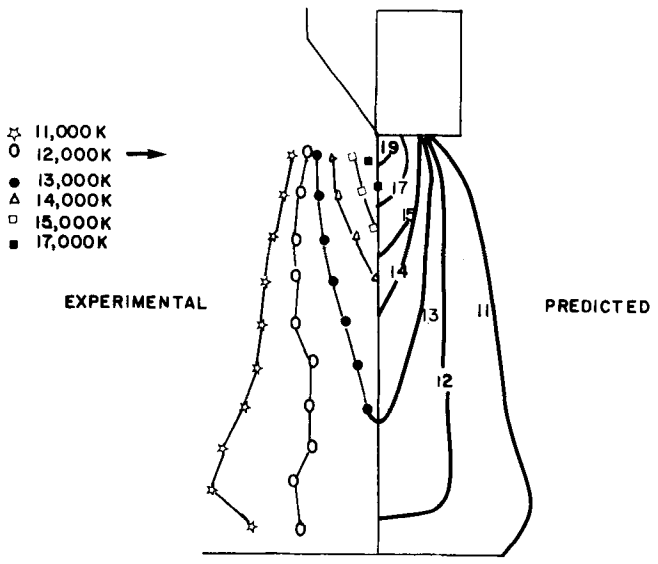

Fig. 5—Comparison between predicted and experimental isotherms for 100 A, 10 mm arc.

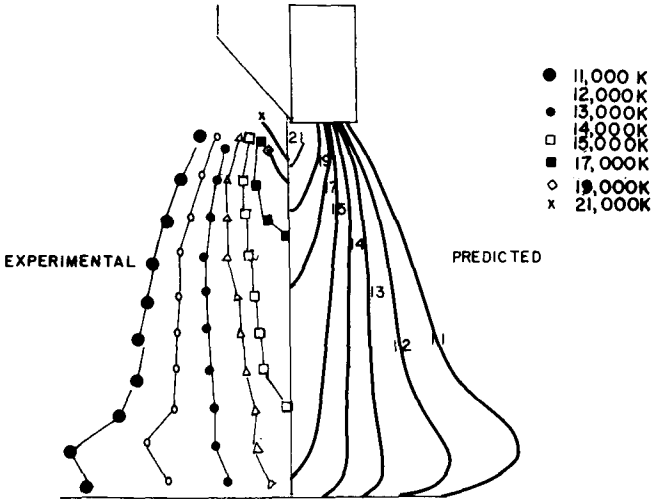

Fig. 6—Comparison between predicted and experimental isotherms for 200 A, 10 mm arc.

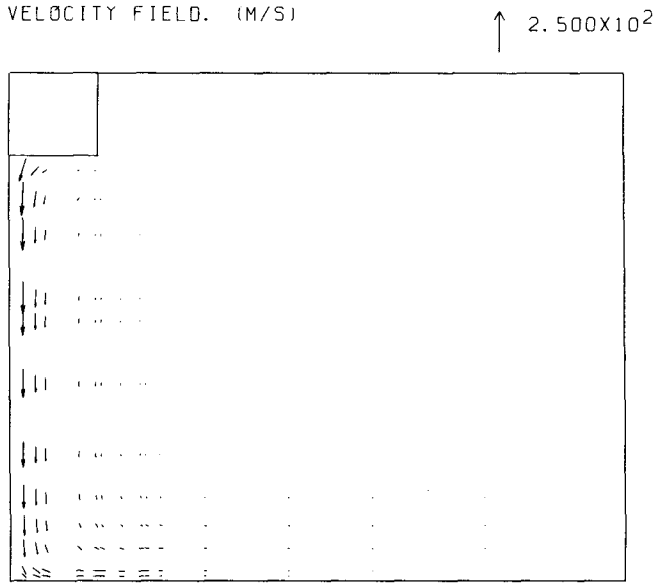

Fig. 8—Predicted velocity field, I = 200 A, L = 10 mm.

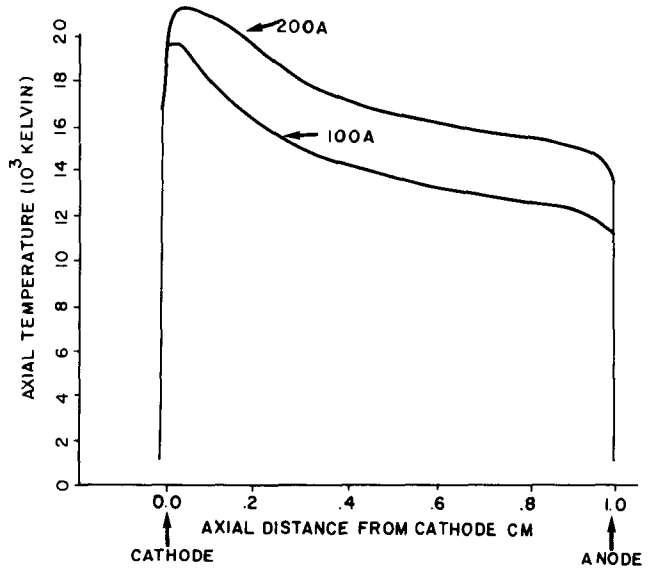

Fig. 7—Axial temperature as a function of the distance from the cathode for two arc currents.

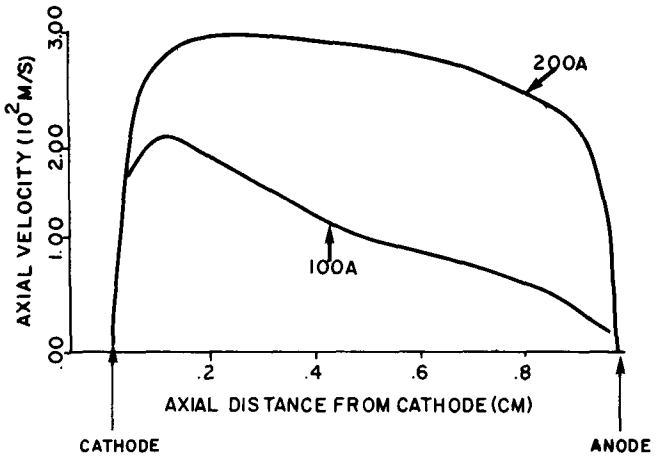

Fig. 9—Predicted axial velocity as a function of the distance from the cathode for two arc currents.

flow of gas from the cathode and its impingement upon the anode. Figure 9 shows the axial variation of plasma velocity for 100 A and 200 A arcs at an arc length of 10 mm.

It should be remarked that the two curves have a markedly different shape, which may be explained by the fact that ratio arc length/cathode spot radius will be smaller for the higher current. Another important point which should be made here is that for the 200 A arc the higher Reynolds number will cause a smaller spread in the velocity field, which may in turn explain practical observations that a disproportionately deeper penetration into the weldpool may occur upon increasing the arc current.

The maximum plasma velocity may be estimated from the simple analytical expression of Maecker[16] which may be written as:

$$u_{max} = \left(\frac{\mu_0}{2\bar{\rho}}\right)^{0.5} R_c J_c \qquad [19]$$

This expression is only very approximate because it assumes a constant radial distribution of current density, a constant arc density $\bar{\rho}$, and neglects the presence of the cathode. Taking a representative arc density of 0.01 kg/m^3, Eq. [19] predicts a maximum velocity of 360 m/s for the 100 A arc and 505 m/s for the 200 A arc. These are considerably higher than the values calculated by the present model (210 m/s and 304 m/s, respectively), but it is interesting to note that the present model obeys the linear relationship (at constant cathode current density) between the maximum velocity and the cathode spot radius. Equation [19] may still be employed to relate the maximum plasma velocity to the arc variables if an adjusted constant is introduced. The amended expression may be written as:

$$u_{max} = \left\{0.17\frac{\mu_0}{\bar{\rho}}\right\}^{0.5} R_c J_c \qquad [20]$$

(iii) *Electromagnetic Field*

The predicted magnetic field and the corresponding current density distribution for a 10 mm 200 A arc are given in

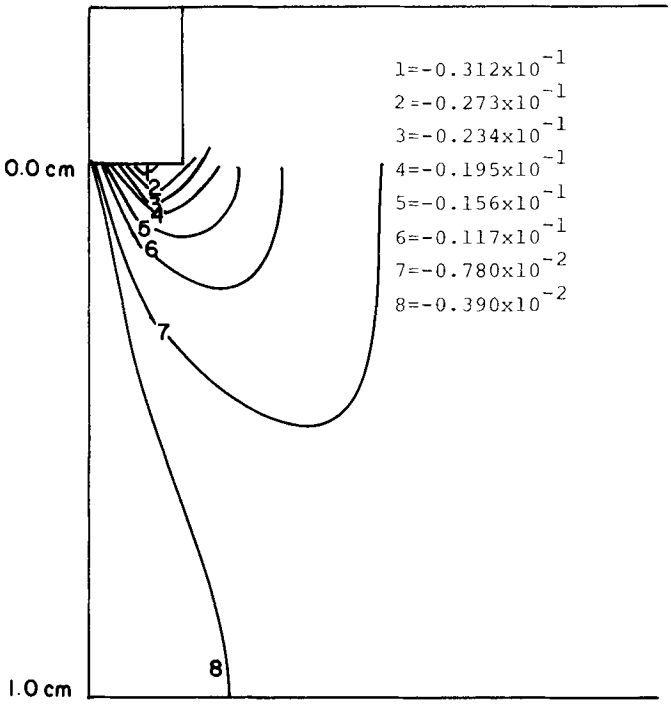

Fig. 10—Predicted azimuthal magnetic field (kg · s^{-2} A^{-1}), I = 200 A, L = 10 mm.

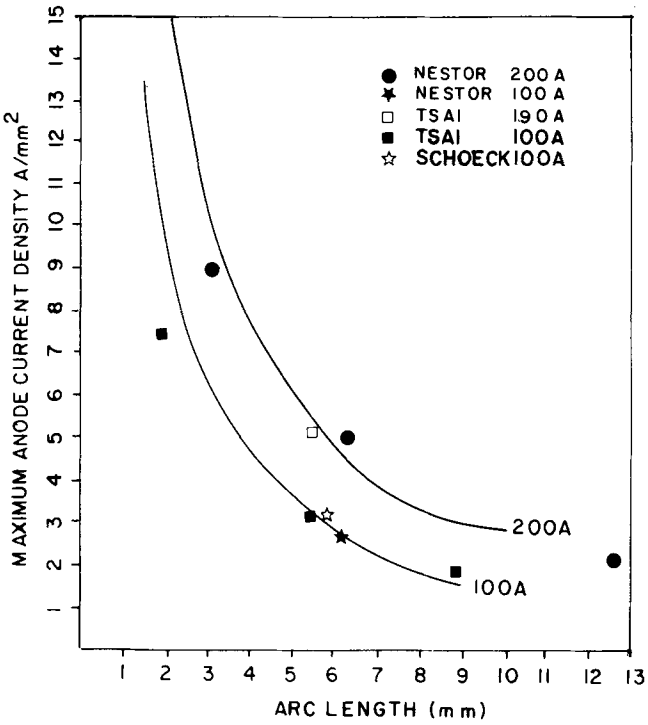

Fig. 12—Comparison between predicted (continuous line) and measured values (discrete data points) of the maximum anode current density as a function of arc length.

Figures 10 and 11, respectively. The divergence of the current in the vicinity of the cathode, which gives rise to the cathode jet, is clearly demonstrated.

(iv) *Anode Current Density*

Figure 12 shows a comparison between the predicted current density at the center of the anode, $J_a(r = 0)$, and those measured by Tsai,[7] Nestor,[15] and Schoeck and Eckert.[17] It is seen that the agreement is quite good.

It was found that the predicted values of the peak current density at the anodes of a series of arcs of different lengths were virtually identical to the axial variation predicted for one long arc. This implies that the presence of the anode has little effect on the current density distribution in the arc. The predicted current/length curves are given in dimensionless form in Figure 13. The dimensionless quantities have been obtained by dividing the current density by the cathode current density, J_c, and the arc length by the cathode spot

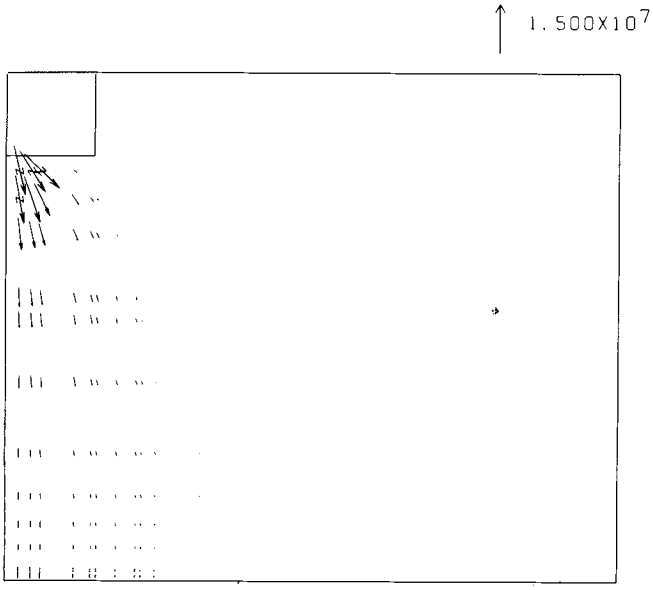

Fig. 11—Predicted distribution of current density (A · m^{-2}), I = 200 A, L = 10 mm.

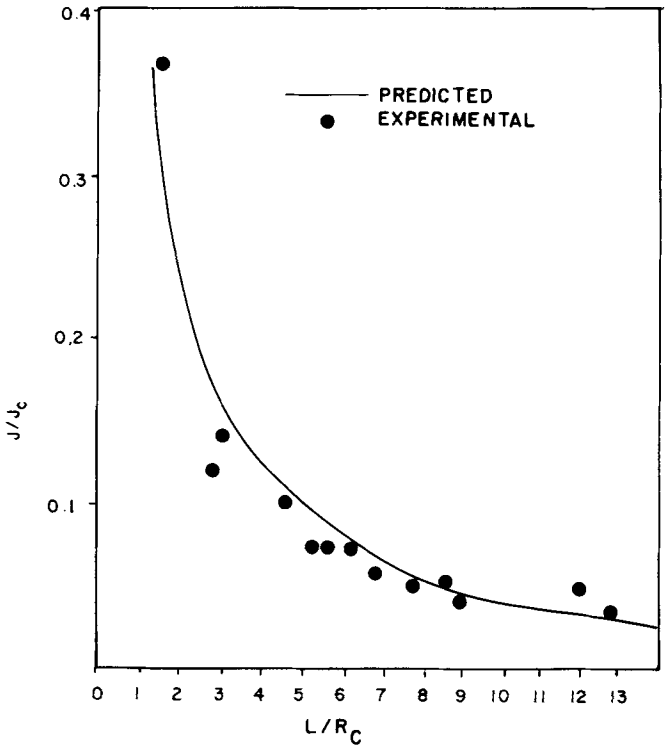

Fig. 13—Maximum anode current density as a function of L/R_c.

radius, R_c. The curves in Figure 12, corresponding to arc currents of 100 A and 200 A, are now coincidental. This implies a relationship of the following form:

$$J_a(r = 0) = f\{L/R_c\}J_c \qquad [21]$$

where J_c is independent of arc current.

Although Eq. [21] is certainly an oversimplification of the real situation, it serves as a useful approximate formula for the arc current density over the restricted range of process parameters encountered in arc welding. Also included in Figure 13 is a collection of experimental data points for arc currents ranging from 50 A to 300 A and, again, it is seen that there is quite good agreement between prediction and measurement.

A comparison between the measured and the predicted radial distributions of the current density is given in Figure 14 for a 6.3 mm arc at 200 A. Again, the predictions agree quite closely with experiment.

(v) *Anode Heat Fluxes*

Figure 15 shows a comparison between the predicted and experimental[7,15,17] values of the heat flux at the center of the anode as a function of dimensionless arc length. The data points are annotated with the arc current/100. Figure 15 also shows the predicted values of the condensation heat flux, $J_a(r = 0)V_w$ and the total electron heat flux $J_a(r = 0)\{V_w + 2.75\}$, since by Eq. [21] both of these quantities are independent of the arc current.

It is evident from Figure 15 that there is considerable scatter in the experimental data, with the measurements of Tsai[7] being somewhat less than those of Schoeck[17] or Nestor,[15] especially at short arc lengths. The predicted heat fluxes are in the correct overall range although it appears that the correlation used in the model somewhat overestimates the convective contribution (which is represented by the vertical displacement of the data points from the broken line in Figure 15). The predictions show an increased convective contribution at shorter arc lengths which is to be expected intuitively. The experimental data, on the other hand, tend to suggest a decreasing importance of convection at short arc lengths, which is difficult to explain unless some other mechanism, *e.g.*, anode vaporization, comes into effect to cool the anode in this region. This, as yet an unresolved problem, will require further attention.

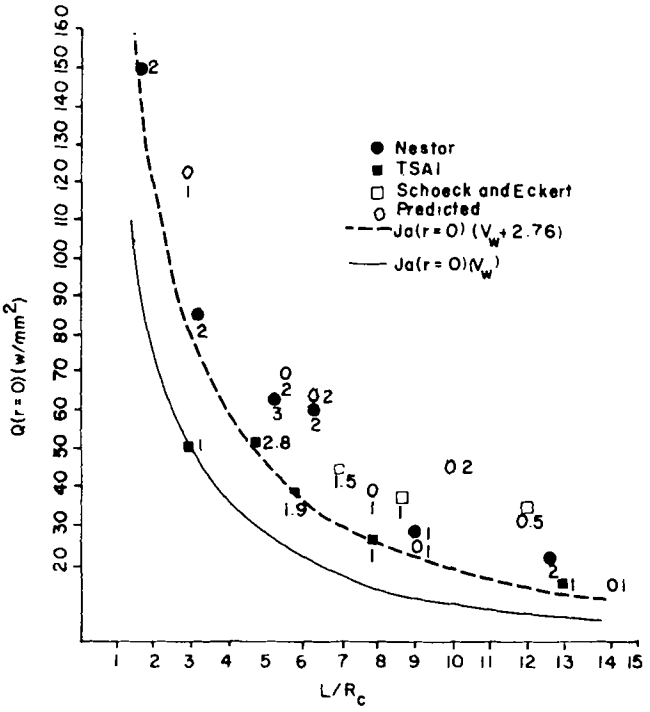

Fig. 15—Comparison between predicted and experimentally measured heat fluxes at the center of the target (annotated with arc current/100).

Figure 16 shows the predicted radial distribution of the various components that make up the overall heat flux for a

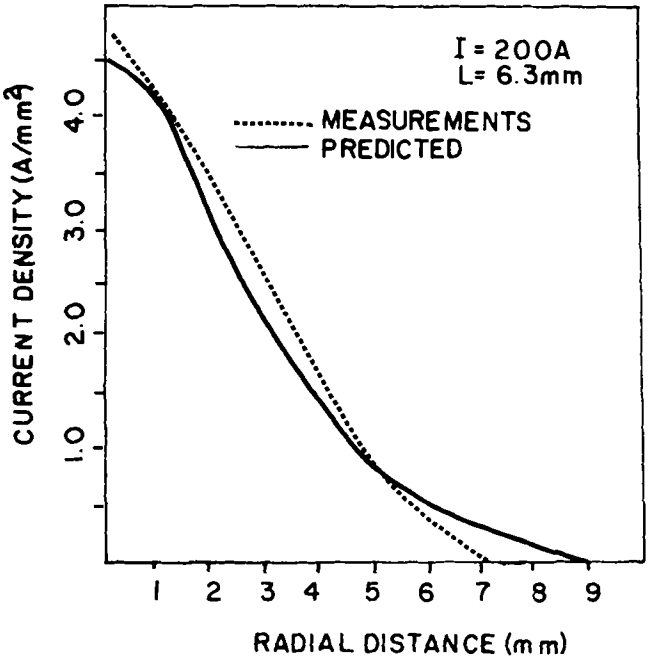

Fig. 14—Comparison between predicted and experimental anode current density, I = 200 A, L = 6.3 mm.

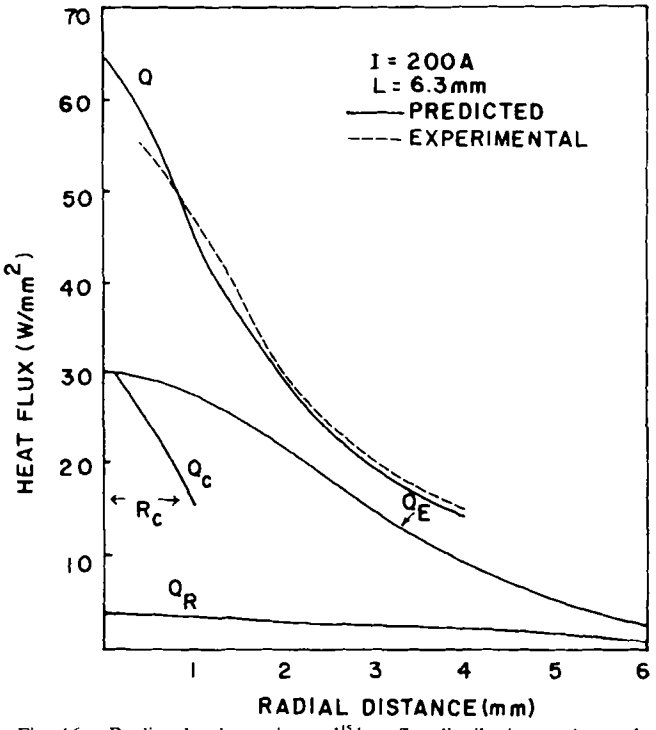

Fig. 16—Predicted and experimental[15] heat flux distributions at the anode.

200 A, 6.3 mm arc together with the experimental measurements of Nestor.[15] It is seen that at the center of the anode the convective term comprises about 46 pct of the total heat flux, and the electronic heat flux contributes about 53 pct. Sanders and Pfender[12] found that the average heat transfer by convection and electron flow for argon arcs in the range from 50 to 350 A was 44 pct and 51 pct, respectively.

It should be noted that the radiative heat flux in Figure 16 is the radiative flux from the plasma incident upon the anode and must be multiplied by the emissivity of the anode to find the amount actually absorbed. In addition, there will be a radiative loss due to emission from the anode.

(vi) *Momentum Transfer to Weldpool*

The shear stress generated by the motion of the plasma past the anode surface results in a transfer of momentum from the plasma to the anode. For solid surfaces this is unimportant but for a weldpool it is possible that it may affect the fluid flow in the pool and, possibly, the structure of the weld.

The shear stress may be written as:

$$\tau_a = \mu_a \cdot \left.\frac{dv}{dn}\right|_{n=0} \qquad [22]$$

where n is normal to the surface.

Figure 17 shows the predicted shear stress at the anode for an arc current of 200 A and arc lengths of 6.2 mm and 10 mm. The stress is zero at the axis of symmetry, where the radial velocity is zero and rises to a maximum at about one cathode spot radius. As expected, the maximum value attained decreases as the arc length is increased. It should be noted that when surface tension gradients exist at the free surface of weldpools (*e.g.*, due to the combination of temperature gradients and the effect of impurities), these could give rise to much higher local values of the shear stress than predicted here. However, in the absence of surface tension gradients the effect of jet momentum calculated here may play a significant role in affecting the flow pattern in the weldpool.

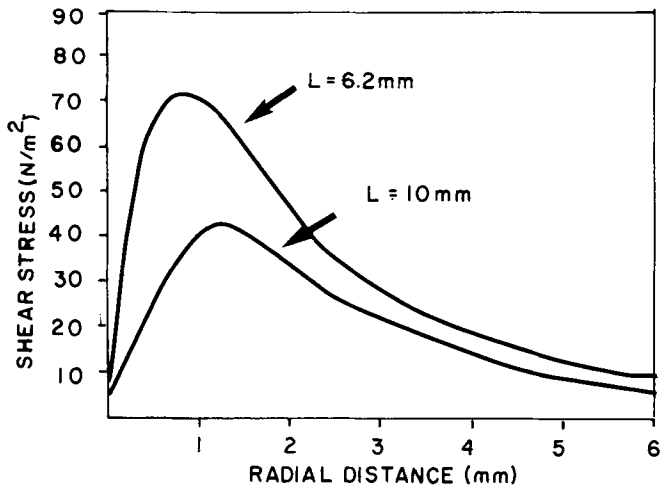

Fig. 17—Radial distribution of shear stress at the anode for a 200 A arc at two different arc lengths.

V. CONCLUDING REMARKS

Through the statement of Maxwell's equations, the laminar Navier-Stokes equations, and the differential thermal energy balance equation a mathematical model has been developed to describe the heat and fluid flow fields in welding arcs. This model represents an extension of previous work reported by this laboratory and by Pfender and coworkers in that particular attention is being paid to the interaction between the plasma and the electrodes. This problem is of considerable practical interest in welding because the definition of the heat flux and current flux impinging on the surface of the weldpool is one of the key problem areas.

Calculations were carried out to represent 100 A and 200 A arcs with various arc lengths for conditions that are considered to be typical for TIG practice.

In comparing the theoretical predictions based on the model with measurements,

1. The predicted temperature fields were found to be in good agreement with spectroscopically measured values.
2. The predicted axial current densities at the anode were found to be in good agreement with experimental data and it was found that the presence of the anode had little effect on the current density in the arc. This implies that the anode current density for a range of arc lengths could be taken directly from the results calculated for a longer arc. The predicted centerline current density for the two arc currents was found to be coincident when presented in dimensionless form.
3. The predicted convective fluxes were in reasonable agreement with experiment although it was impossible to make a totally critical comparison due to the large scatter in the experimental data.

The quantitative representation of the arc thus obtained should pave the way toward the development of a comprehensive mathematical model of the arc welding process where the interaction between the pool and the arc regions is properly covered.

SYMBOLS

B	magnetic field vector
B	azimuthal component of magnetic field
C_p	specific heat
e	electronic charge
F	Lorentz force per unit volume
h	plasma enthalpy
I	arc current
J	current density vector
k_B	Boltzmann's constant
k	thermal conductivity
P	pressure
Q	total heat flux to anode
Q_c	convective heat flux to anode
Q_E	electron heat flux at anode
Q_r	heat flux at anode due to radiation from the arc
r	radial coordinate
R_c	cathode spot radius
S_r	radiation loss per unit volume from arc
S_t	source term for energy equation
T	temperature

u axial velocity
v radial velocity
V voltage
z axial coordinate
α Prandtl number
μ viscosity
μ_0 permitivity of free space
ρ density
σ electrical conductivity of plasma
τ shear stress
ϕ coefficient of thermal diffusion of electrons

Subscripts

a anode or anode fall
b edge of boundary layer in plasma
c cathode or cathode fall
e electron
E electronic
max maximum value on arc axis
r the radial direction
w work function
z the axial direction

ACKNOWLEDGMENTS

The authors wish to thank the United States Army Research for support of the study under Grant No. DAAG29-83-K-0022, and Office of Naval Research for support under Grant No. N00014-84-K-042.

REFERENCES

1. G. Oreper and J. Szekely: *Jnl. Fluid Mech.*, in press.
2. M. Ushio, J. Szekely, and C. W. Chang: *Ironmaking and Steelmaking*, 1981, vol. 8, pp. 279-86.
3. J. W. McKelliget and J. Szekely: *Jnl. Phys. D: Appl. Phys.*, 1983, vol. 16, pp. 1007-22.
4. J. Szekely, J. McKelliget, and M. Choudhary: *Ironmaking and Steelmaking*, 1983, vol. 10, pp. 169-79.
5. K. Hsu, K. Etemadi, and E. Pfender: *Jnl. Appl. Phys.*, 1983, vol. 54, pp. 1293-1301.
6. K. Hsu and E. Pfender: *Jnl. Appl. Phys.*, 1983, vol. 54, pp. 4359-66.
7. N. Tsai: Ph.D. Thesis, Dept. Materials Science and Engineering, Massachusetts Institute of Technology, Cambridge, MA, 1983.
8. D. C. Evans and R. S. Tankin: *Phys. Fluids*, 1967, vol. 10, pp. 1137-44.
9. C. F. Liu: Ph.D. Thesis, Dept. of Mechanical Engineering, University of Minnesota, Minneapolis, MN, 1977.
10. K. C. Hsu and E. Pfender: *Jnl. Appl. Phys.*, 1983, vol. 54, pp. 3818-24.
11. H. A. Dinulescu and E. Pfender: *Jnl. Appl. Phys.*, 1980, vol. 51, pp. 3149-57.
12. N. A. Sanders and E. Pfender: *Jnl. Phys.*, 1984, vol. 55, pp. 714-22.
13. W. M. Rosenhow and J. P. Hartnett: *Handbook of Heat Transfer*, McGraw-Hill, New York, NY, 1973, pp. 8-126.
14. W. Pun and D. B. Spalding: Report No. HTS/76/2, Heat Transfer Section, Imperial College, London, 1976.
15. O. H. Nestor: *Jnl. Appl. Phys.*, 1962, vol. 33, pp. 1638-48.
16. H. Maecker: *Z. Phys.*, 1955, vol. 141, pp. 198-216.
17. P. Schoeck and E. R. G. Eckert: *5th Int. Conf. Phen. Ionized Gases*, Munich, 1961, vol. 2, pp. 1812-29.